



Theoretical Anti-Corrosion Study for Synthesis of Two New Thiazole Derivatives

Pelin Koparir

Firat University Department of Chemistry, Faculty of Science, 23169, Elazig, Turkey

E-mail: mpelin23@hotmail.com

ABSTRACT

Two newly thiazole (1-(4-(3-methyl-3-phenylcyclobutyl)thiazol-2-yl)-3-(4-nitrophenyl)thiourea and 1-(4-methoxyphenyl)-3-(4-(3-methyl-3-phenylcyclobutyl)thiazol-2-yl)thiourea were synthesise. The molecular formula was characterized using Fourier-Transform Infrared (FT-IR) spectroscopy and Nuclear Magnetic Resonance (NMR). Theoretical vibration was calculated using Gaussian 09W software, and corrosion inhibiting activity was calculated using quantum chemical calculations. Furthermore, the GaussView 5.0 package on the B3LYP/6-311G(d,p) method was used to calculate the energy of the highest occupied molecular orbital (E_{HOMO}), the energy lowest unoccupied molecular orbital (E_{LUMO}) the energy gap ($E = E_{\text{LUMO}} - E_{\text{HOMO}}$), the dipole moment (μ), and the percent of transmitted electrons (ΔN). Based on the results of inhibitor activity, other molecular properties such as hardness (η), softness (σ), and electronegativity (χ) were calculated. Quantum chemical calculations were used to predict the corrosion inhibiting activities of the derivatives. As a result, the corrosion inhibitor behavior can be predicted without an experimental study. The results show a strong relationship between organic-based corrosion inhibitors and the process's quantum chemical parameters.

ARTICLE INFO

Keywords:

Organic Synthesis
Thiazol
Derivative
DFT
Electronic Properties
Inhibitor Activity

Received: 2022-05-25

Accepted: 2022-06-14

ISSN: 2651-3080

DOI: 10.54565/jphcfum.1121438

Introduction

Thiazoles are azole derivatives (including imidazoles and oxazoles) with the molecular formula C_3H_3NS and atoms arranged in five aromatic rings [1, 2]. The odor of thiazole is similar to that of pyridine, and the liquid is light yellow colors. Thiazoles are used to obtain free carbon particles and then react with transition metals to form a complex [3-6]. Nitrogen atoms have the highest negative charge in the molecular formula in a thiazole, followed by carbon and sulfur atoms [7]. Furthermore, thiazoles have been shown to have potential pharmacological activities [8], for example, they are the best heterocycle compounds to begin synthesizing new drugs [9]. Thiazole has been targeted in the industry because their Schiff base complexes have different chemical activities such as catalytic activation [10, 11], photochromic features [12], electrochemical transfer [13], and formation of a complex for several toxic metals [14]. On the other hand, other organic compounds were not directly used due to economic considerations.

Cyclobutanes have been known for more than a century as intriguing structural motifs, but they have received far less attention than their homologs [15]. The synthesis of cyclobutane rings particularly stereospecifically, poses significant challenges in synthetic chemistry due to the

highly strained ring topologies. Cyclobutanes have increased stability of the structures could appear in a wide range of complex natural products, rather than just man-made molecules [16]. Natural products containing cyclobutane are particularly appealing targets for total synthesis due to their novel chemical structures and high biological activity. Cyclobutanes, on the other hand, readily undergo several ring-opening reactions due to their proclivity to release inherent strain energies [17].

Organic compounds with cyclic structures containing heteroatoms (oxygen, nitrogen, sulfur, and phosphorus) and a conjugate bond have higher inhibitor activity [18-20]. Inhibitory activities are carried out by electrons and dissociated electron pairs in their molecular structure. The presence of atoms such as N, O, S, and C=N groups in a heterocyclic molecule is thought to have high anti-corrosion activity [21, 22].

DFT has a good cost-accuracy ratio for large systems, but the calculations are typically prohibitive in terms of computational effort, and it works better for charged systems (e.g., proteins with charged residues) [23-25]. Theoretical computation methodologies have grown in popularity for theoretical modeling and the design of functional materials such as pharmaceutical substances

[26]. A computational chemistry method is a promising tool for identifying corrosion inhibitors because it interprets inhibitory activity using a number of quantum chemical features [27, 28]. Quantum chemistry properties are frequently used in theoretical corrosion research and are classified into three types: energy, molecular orbital energy, and atomic charges [29]. The inhibitor activity is closely related to several parameters, including E_{HOMO} , E_{LUMO} energy, softness, and hardness [30, 31]. The density Function Theory (DFT) has been widely used to calculate a molecule's total electron energy based on its electron density [32, 33].

A thiazole ring is an electron-rich system that can easily form hydrogen bonds between molecules with materials in different species. Compounds containing thiazole have been reported to be an inhibitor of broad-spectrum [34, 35]. For this purpose, two new compounds (IIIa,b) of the thiazole series containing cyclobutane derivatives with thiourea which are not found in the literature were synthesized. FT-IR and NMR were used to determine the chemical structure of the derivatives, and DFT methods were used to explain corrosion inhibitor activity.

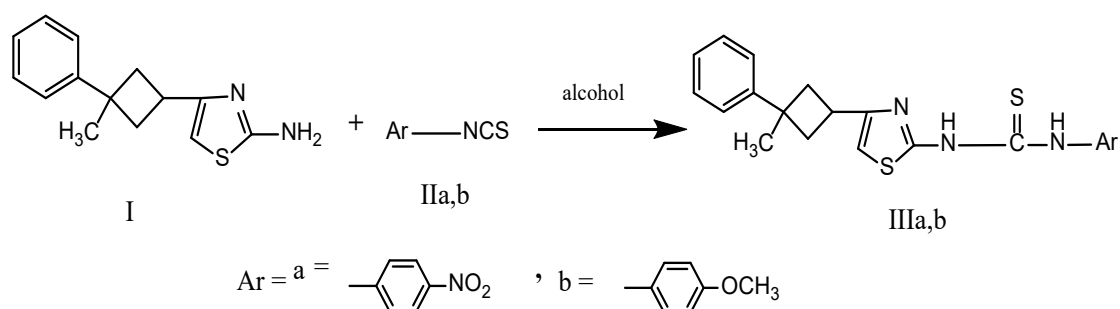


Fig. 1 The methodical approach to synthesizing thiazole derivatives.

Synthesis 1-(4-(3-methyl-3-phenylcyclobutyl)thiazol-2-yl)-3-(4-nitrophenyl)thiourea (IIa)

4-[1-Phenyl-1-Methyl-1-Cyclobutan-3-yl]-2-aminothiazole, 2.44 g (0.01 mol), CaCl_2 and thermometer were arranged in a 3-mouth reaction flask, the thiazole (0.01 mol) and 4-Nitrophenyl isocyanate were calculated (0.01 mol) was placed in the reaction flask. Absolute ethyl alcohol 65 ml was added. The reaction was continued for 1 hour at room temperature. It was refluxed for 12 hours under reflux. After IR control 3280-320 cm^{-1} NH peak and 1360-1340 cm^{-1} C=S peaks were observed, the reaction was stopped. It was cooled and filtered, the filtrate was washed with water and the ether phase was extracted. It was dried with MgSO_4 , filtered. Dissolved in chloroform then solvent was removed in the evaporator, precipitated in n-hexane, dried in open air and crystallized in ethanol. Yield 71%, Melting point: 274. The molecular characteristics of 1-(4-(3-methyl-3-phenylcyclobutyl)thiazol-2-yl)-3-(4-nitrophenyl)thiourea (I) summarized below:

IR (cm^{-1} , KBr): (3280-3200) (ν N-H), 3107 cycloalkane (ν C-H), 3055 Aromatic (ν C-H), 2980-2870 Aliphatic (ν C-H), 1600-1590 (ν C=N), 1360-1340 (ν C=S), 1159-1000 (ν C-N), 690-655 (ν C-S-C). $^1\text{H-NMR}$ (200 MHz, CDCl_3 , ppm, δ), 10.46-10.06 (br, 2H, 2xNH), 7.55-7.12(m, 9H, Aromatic protons), 6.42 (s, 1H, CH=, in thiazole), 3.73-3.60 (p, 1H, methine proton in the Cyclobutane ring), 2.68-2.46 (m, 4H, CH_2 protons in Cyclobutane), 1.56 (s, 3H, CH_3 protons). $^{13}\text{C-NMR}$ (200 MHz, CDCl_3 , ppm),

Materials and Methods

4-[1-Phenyl-1-Methyl-1-Cyclobutan-3-yl]-2-aminothiazole we got from Firat University organic chemistry Lab. Calcium chloride (CaCl_2) (CAS- 10035-04-8 Istanbul), Thiazole ($\text{C}_3\text{H}_3\text{NS}$) (CAS- 288-47-1 Istanbul), 4-Nitrophenyl isocyanate ($\text{O}_2\text{NC}_6\text{H}_4\text{NCO}$) (CAS- 100-28-7 Istanbul), Ethyl alcohol ($\text{CH}_3\text{CH}_2\text{OH}$) (CAS- 64-17-5 Istanbul), Magnesium sulfate (MgSO_4) (CAS- 7487-88-9 Istanbul), n-Hexane ($\text{CH}_3(\text{CH}_2)_4\text{CH}_3$ Istanbul) (CAS- 110-54-3 Istanbul), 4-Methoxyphenyl isocyanate ($\text{CH}_3\text{OC}_6\text{H}_4\text{NCO}$) (CAS- 5416-93-3 Istanbul). All chemicals were purchased from Merck or Aldrich, used without further purification. Two novel thiazole of 1-(4-(3-methyl-3-phenylcyclobutyl)thiazol-2-yl)-3-(4-nitrophenyl)thiourea and 1-(4-methoxyphenyl)-3-(4-(3-methyl-3-phenylcyclobutyl)thiazol-2-yl)thiourea synthesized, as show in Figure 1. The melting point of the derivatives was measured by Gallenkamp digital melting point. $^1\text{H NMR}$ and $^{13}\text{C NMR}$ spectra were recorded on an FX 90 JEOL 200 MHz $^1\text{H NMR}$ and Varian Gemini 100 MHz for ^{13}C , using CDCl_3 as a solvent.

178.22(C=S, Cs), 163.11 (C-2 in Thiazole), 157.09 (Aromatic Quaternary C's), 153.81 (C-4 in Thiazole), 140.79, 131.41, 130.30, 127.84, 126.49, 125.47 (Aromatic C's), 106.56 (C-5 in Thiazole), 42.73, 40.93 (Cyclobutane (CH_2) Cs), 32.61, (Cyclobutane CH); 32.03 (CH_3). Elemental Analysis results; Theoretical/Experimental C: 59.41/59.40, H:4.75/4.79, N:13.20/13.13, S: 15.11/15.00, $\text{C}_{21}\text{H}_{20}\text{N}_4\text{O}_2\text{S}_2$ M.wt:424 g/mol.

Synthesis 1-(4-methoxyphenyl)-3-(4-(3-methyl-3-phenylcyclobutyl)thiazol-2-yl)thiourea (IIIb)

4-[1-Phenyl-1-Methyl-1-Cyclobutan-3-yl]-2-aminothiazole, 2.44 g (0.01 mol), CaCl_2 and thermometer were arranged in a 3-mouth reaction flask, and thiazole (0.01 mol) and 4-Methoxyphenyl isocyanate were calculated (0.01 mol) and was placed in the reaction flask. Absolute ethyl alcohol 65 ml was added. The reaction was continued for 1 hour at room temperature. It was refluxed for 12 hours under reflux. After IR control 3280-320 cm^{-1} NH peak and 1360-1340 cm^{-1} C=S peaks were observed, the reaction was stopped. It was cooled and filtered, the filtrate was washed with water and the ether phase was extracted. It was dried with MgSO_4 , filtered. Dissolved in chloroform then solvent was removed in the evaporator, precipitated in n-hexane, dried in open air and crystallized in ethanol. Yield 64% Melting point: 273. The molecular characteristics of 1-(4-methoxyphenyl)-3-(4-(3-methyl-3-

phenylcyclobutyl)thiazol-2-yl)thiourea (II) summarized below:

IR (cm⁻¹, KBr): 3280-3200 (νN-H), 3107 cycloalkane (νC-H), 3055 Aromatic (νC-H), 2980-2870 Aliphatic (νC-H), 1600-1590 (νC=N), 1360-1340 (νC=S), 1159-1000 (νC-N), 690-655 (νC-S-C). ¹H-NMR (200 MHz, CDCl₃, ppm, δ), 13.01-12.72 (br, 2H, 2xNH), 7.47-6.81(m, 9H, Aromatic protons), 6.37 (s, 1H, CH= in thiazole), 3.79-3.31 (m, 3H, O-CH₃ and 1H methine proton in the Cyclobutane ring), 2.55-2.45 (m, 4H, CH₂ protons in Cyclobutane), 1.51 (s, 3H, CH₃ protons). ¹³C-NMR (200 MHz, CDCl₃, ppm), 178.28(C=S, Cs), 163.53 (C-2 in Thiazole), 157.16, 157.12 (Aromatic Quaternary C'u), 153.81 (C-4 in Thiazole), 140.79, 131.41, 130.30, 127.84, 126.49, 125.47 (Aromatic C's), 106.56 (C- in Thiazole 5), 57.14(O-CH₃, C10), 42.73, 40.93 (Cyclobutane (CH₂)₂ Cs); 32.61, (Cyclobutane CH); 32.01 (CH₃). Elemental Analysis results; Theoretical/Experimental C: 64.52/64.50, H:5.66/5.66, N:10.26/10.24, S:15.66/15.65, C₂₂H₂₃N₃OS₂ Ma:409 g/mol.

Computational Methods

The molecular geometry of the thiazole derivatives was obtained using the GaussView 5.0 package, which contains molecular imaging software that explains the geometry of molecules in the gas phase. Gaussian 09W software was used to calculate the molecule structure [36, 37]. DFT is suitable for workstation capability in the Gaussian09W program at the basis set 6-311G(d,p). It has significantly improved against Hartree-Fock. DFT is typically faster than Hartree-Fock techniques, with comparable results

[38]. Larger basis sets should produce better and thus more accurate results as they approach the infinite basis set limit. A constricted Gaussian basis set (6-311G) is generated for the ground states of first row atoms by optimizing exponents and coefficients at the Møller–Plesset (MP) second-order level. There is a threefold split in the valence S and P shells, as well as a single set of uncontracted polarization functions, on each atom. The functions in parenthesis "(d)" or "(d,p)" are polarization functions, which are used to precisely define chemical bonds (higher angular momentum than the valence orbitals). If there is no comma, as in (d), you are including polarization functions in all heavy atoms (except hydrogen), whereas if there is a comma, as in (d,p), you are including the first functions in heavy atoms and the second ones in hydrogen atoms [39].

DFT was used to calculate the electron density and other electronic properties of E_{HOMO} (higher occupational molecular orbital), E_{LUMO} (lowest occupational molecular orbital), ΔE (energy bandgap), (electronegativity) χ, (hardness) η, (softness) σ, (electrophilicity index) ω, (nucleophilicity index) ε, (Chemical potential) Pi, (dipole moment) μ, and (fraction of transferred electrons) ΔN. The HOMO, LUMO, and μ of the molecule are calculated in Gaussian from the output file, while other parameters are calculated using standard equations. The E_{HOMO} and E_{LUMO} values are correlated to their ionization energy and electron affinity values, according to Koopman's theorem [40, 41]. The following equations were used to calculate the other parameters:

$$I = -E_{\text{HOMO}} \quad [41] \quad (1)$$

$$A = -E_{\text{LUMO}} \quad [41] \quad (2)$$

$$\Delta E = (E_{\text{LUMO}} - E_{\text{HOMO}}) \quad [42] \quad (3)$$

$$\eta = (I - A) / 2 \quad [43] \quad (4)$$

$$\sigma = 1/\eta \quad [44] \quad (5)$$

$$\chi = (I + A) / 2 \quad [45] \quad (6)$$

$$Pi = -\chi \quad [45] \quad (7)$$

$$\omega = Pi^2/2\eta \quad [46] \quad (8)$$

$$\varepsilon = Pi * \eta \quad [47] \quad (9)$$

The electrophilicity index (ω) (equation 8) was depleted as a result of electrons moving from transmitter to receiver. The nucleophilicity index (ε) (equation 9) is a new chemical structure identifier. (ΔN) represents the number of electrons exchanged between the inhibitor and the metal.

$$\Delta N = \frac{\chi_{\text{metal}} - \chi_{\text{inhibitor}}}{2(\eta_{\text{metal}} - \eta_{\text{inhibitor}})} \quad [48] \quad (10)$$

The χ inhibitor and η inhibitor values in the equation are determined theoretically, and Pearson [50] experimentally calculates the χ and η for metals. According to Pearson, η for metal are zero, and ionization potential (I) with electron affinity (A) for a single metal is equal (I = A).

Results and Discussion

Spectroscopy Analysis

The theoretical vibrational frequencies for our products were predicted using B3LYP/6-311(d,p). The vibrational band assignments were used to create the molecular visualization. To encourage the assignment of the observed peaks, we measured the theoretical vibrational frequencies of thiazole derivatives (IIIa and IIIb) and compared them to their experimental results, as shown in Fig. 2. In general, the results of this study's experimental data and theoretical results are comparable. For both compounds, the N-H stretching vibration was observed in the 3280-3200 cm⁻¹ range. For both compounds (IIIa and IIIb), the peak for (νC-H) in cycloalkane was detected at 3107 cm⁻¹.

The (ν C-H) vibration peaks for aromatic and aliphatic were observed at 3055, 2980-2870 cm^{-1} respectively. In both IIIa and IIIb derivatives of thiazole the peaks for (ν C=N), (ν C=S), (ν C-N), (ν C-S-C), were found in a range 1600-1590, 1360-1340, 1159-1000, 690-655 individually. In the FT-IR vibration analysis, there is no identical peaks were found between IIIa and IIIb. All FT-IR peaks for both derivatives are observed in very close ranges.

In $^1\text{H-NMR}$ spectra, the N-H proton peak for IIIa appeared at 10.46-10.06 ppm (br, 2H, 2xNH), while for IIIb was appeared at 13.01-12.72 ppm. Protons in aromatic (m, 9H, Aromatic protons) were found to be 7.55-7.12 ppm for IIIa, and the same peaks for IIIb were found at 7.47-6.81 ppm. In the IIIa compound at 6.42 ppm a single proton peak for thiazole was observed, while the same peak for IIIb was found at 6.37 ppm. The peaks for cyclobutane ring (p, 1H, methine proton in the), Cyclobutane (m, 4H,

CH₂ protons in), and CH₃ protons (s, 3H,) in Derivative IIIa were observed at 3.73-3.60, 2.68-2.46, and 1.56 ppm, while the peaks for derivative IIIb was observed at 3.79-3.31, 2.55-2.45, and 1.51 ppm respectively.

In $^{13}\text{C-NMR}$ spectra, the Cs for C=S and C-2 for thiazole has been observed at 178.22, 163.11 ppm for compound IIIa, and compound IIIb has been observed at 178.28 and 163.53 ppm. For the derivative IIIa and IIIb the Aromatic Quaternary C's were found at 157 ppm. The (C-4) in Thiazole for both IIIa and IIIb were detected at 153.81 ppm. The peaks for (C-5) thiazole, (Cyclobutane (CH₂)₂ Cs), (Cyclobutane CH), and (CH₃) for IIIa were found at 106.56, 42.73, 40.93, 32.61, and 32.03, the same peaks for IIIb were detected at 106.56, 42.73, 40.93, 32.61, and 32.01 ppm. There is one identical peak for the derivative IIIb at 57.14 ppm, which is a peak for (O-CH₃, C10), and this peak was not found for the compound IIIa.

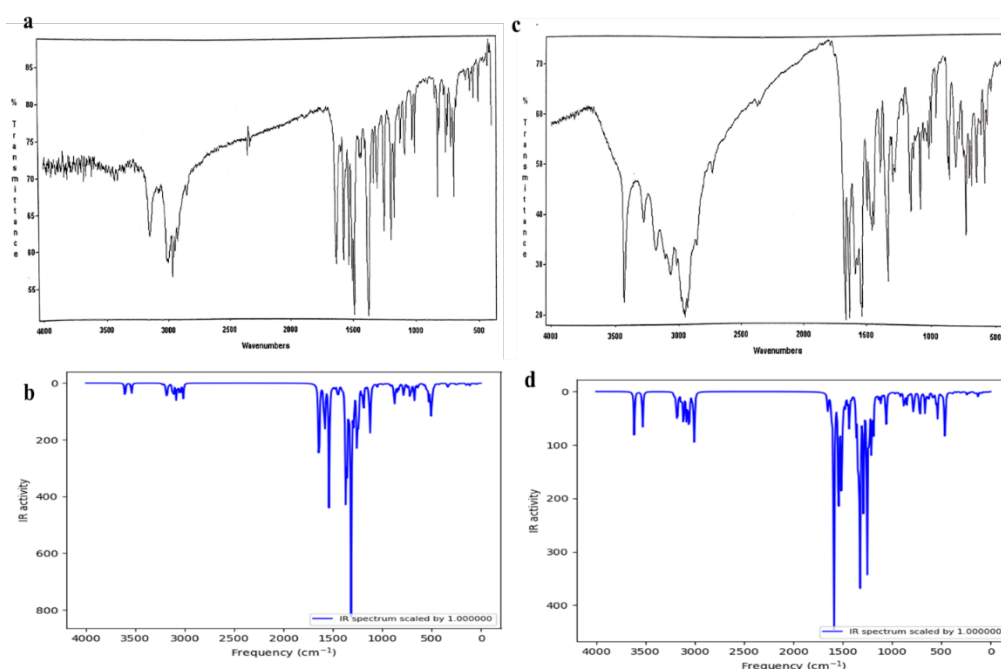


Fig. 2 Shows FT-IR spectra. a) Experimentally vibration for IIIa, b) Theoretically vibration for IIIa, c) Experimentally vibration for IIIb, d) Therotically vibration for IIIb.

Geometrical Optimization

In the gas phase, geometrical optimization for both derivatives (IIIa and IIIb) were investigated using B3LYP/6-311 (d,p). Fig. 3 depicts the molecular structure with assigned atomic numbering in the theoretical

geometric structure, Also Tables 1 and 2 show the bond length, bond angle, and dihedral angles for all atoms without hydrogen. In all measurement methods, normal mode analysis did not yield any negative frequencies for any of the structures.

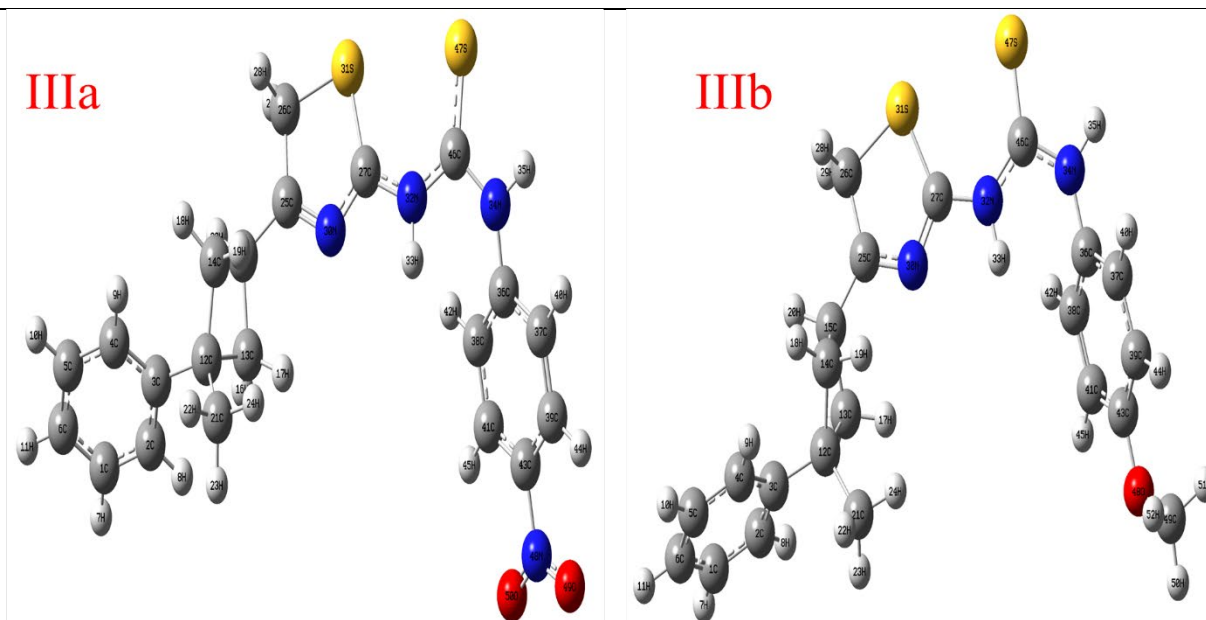


Fig. 3 Geometrical molecular optimization for IIIa and IIIb in the gas phase at the DFT/B3LYP theoretical stage using the 6-311G basis set (d,p).

Table 1. The geometrical optimization (Bond Length, Bond angle, and Dihedral angle) for the compound IIIa

Symbol	Bond Length	Symbol	Bond Angle	Symbol	Dihedral Angle
C2-C1	1.3932053	C3-C2-C1	121.246225	C4-C3-C2-C1	0.8955641
C3-C2	1.4000908	C4-C3-C2	117.724555	C5-C4-C3-C2	-0.908545
C4-C3	1.4003733	C5-C4-C3	121.260683	C6-C1-C2-C3	-0.2387198
C5-C4	1.3930396	C6-C1-C2	120.259316	C12-C3-C2-C1	176.3340147
C6-C1	1.3923465	C12-C3-C2	121.105777	C13-C12-C3-C2	42.2336023
C12-C3	1.5273475	C13-C12-C3	114.294882	C14-C12-C3-C2	140.8834021
C13-C12	1.5655663	C14-C12-C3	113.955514	C15-C13-C12-C3	98.1709296
C14-C12	1.5654533	C15-C13-C12	89.9692486	C21-C12-C3-C2	-88.6157831
C15-C13	1.5482154	C21-C12-C3	109.429334	C25-C15-C13-C12	139.0845082
C21-C12	1.5344394	C25-C15-C13	119.411933	C26-C25-C15-C13	162.295255
C25-C15	1.4874069	C26-C25-C15	121.482437	C27-C25-C15-C13	-24.804326
C26-C25	1.5116566	C27-C25-C15	155.727531	N30-C25-C15-C13	-20.692989
C27-C25	2.2192029	N30-C25-C15	122.572134	S31-C27-C25-C15	-172.9248594
N30-C25	1.3195842	S31-C27-C25	83.7593537	N32-C27-C25-C15	10.769539
S31-C27	1.7697791	N32-C27-C25	149.907596	N34-N32-C27-C25	167.5012585
N32-C27	1.3784965	N34-N32-C27	164.243487	C36-N3-N32-C27	-146.3555507
N34-N32	2.3104248	C36-N3-N32	100.967244	C37-C36-N34-N32	-145.8061993
C36-N3	1.3982482	C37-C36-N34	117.751573	C38-C36-N34-N32	36.5312208
C37-C36	1.407958	C38-C36-N34	123.204169	C39-C37-C36-N34	-178.4310678
C38-C36	1.4074468	C39-C37-C36	120.769342	C41-C38-C36-N34	178.9400149
C39-C37	1.3828449	C41-C38-C36	120.194226	C43-C41-C38-C36	-0.7212415
C41-C38	1.386913	C43-C41-C38	119.633938	C46-N32-C38-C25	177.6672646
C43-C41	1.3904781	C46-N32-C38	131.337337	S47-C46-N32-C27	7.7565456
C46-N32	1.3622795	S47-C46-N32	125.518943	N48-C43-C41-C38	179.9349961
S47-C46	1.6712104	N48-C43-C41	119.394717	O49-N48-C43-C41	178.653971
N48-C43	1.4695583	O49-N48-C43	117.589992	O50-N48-C43-C41	-1.3788136
O49-N48	1.2253791	O50-N48-C43	117.636091		
O50-N48	1.225385				

Table 2. The geometrical optimization (Bond Length, Bond angle, and Dihedral angle) for the compound IIIb

Symbol	Bond Length	Symbol	Bond Angle	Symbol	Dihedral Angle
C2-C1	1.3931632	C3-C2-C1	121.2633006	C4-C3-C2-C1	0.8460695
C3-C2	1.40036	C4-C3-C2	117.6963692	C5-C4-C3-C2	-0.8438345
C4-C3	1.4003649	C5-C4-C3	121.2781319	C6-C1-C2-C3	-0.2429447
C5-C4	1.3931299	C6-C1-C2	120.2589809	C12-C3-C2-C1	176.3983798
C6-C1	1.3925032	C12-C3-C2	121.0665538	C13-C12-C3-C2	42.9320256
C12-C3	1.527347	C13-C12-C3	114.1926884	C14-C12-C3-C2	141.3567517
C13-C12	1.5647646	C14-C12-C3	114.0791945	C15-C13-C12-C3	97.8780719
C14-C12	1.5644836	C15-C13-C12	89.9500952	C21-C12-C3-C2	-87.9225665
C15-C13	1.5552293	C21-C12-C3	109.3590302	C25-C15-C13-C12	139.5767404
C21-C12	1.5347518	C25-C15-C13	119.0749653	C26-C25-C15-C13	142.6372846
C25-C15	1.4881199	C26-C25-C15	122.5612287	C27-C25-C15-C13	-42.6296061
C26-C25	1.5107695	C27-C25-C15	154.5119572	N30-C27-C25-C15	4.5256373
C27-C25	2.221804	N30-C27-C25	33.109582	S31-C27-C25-C15	-175.0202814
N30-C27	1.3210117	S31-C27-C25	83.5701005	N32-C27-C25-C15	7.6760774
S31-C27	1.7744524	N32-C27-C25	150.4938646	N34-N32-C27-C25	173.2945179
N32-C27	1.3822927	N34-N32-C27	164.1281958	C36-N34-N32-C27	-166.374297
N34-N32	2.3004134	C36-N34-N32	96.1246167	C37-C36-N34-N32	-121.9768239
C36-N34	1.4236829	C37-C36-N34	119.7832969	C38-C36-N34-N32	60.7704051
C37-C36	1.3941436	C38-C36-N34	121.2857072	C39-C37-C36-N34	-177.0680064
C38-C36	1.4036791	C39-C37-C36	120.9975528	C41-C38-C36-N34	178.4141649
C39-C37	1.3939662	C41-C38-C36	120.4397655	C43-C39-C37-C36	-1.2850209
C41-C38	1.3848235	C43-C39-C37	119.7997064	C46-N32-C27-C25	179.0118972
C43-C39	1.3979202	C46-N32-C27	131.3237618	S47-C46-N32-C27	3.7747161
C46-N32	1.3644097	S47-C46-N32	125.0756982	O48-C43-C39-C37	-179.2712895
S47-C46	1.6781846	O48-C43-C39	124.8193539	C49-O48-C43-C39	0.017306
O48-C43	1.3593765	C49-O48-C43	118.6216273		
C49-O48	1.4223042				

Inhibitor Activity

Table 3 summarizes the HOMO and LUMO energies. For derivative IIIb, HOMO and LUMO have more energy than derivative IIIa. HOMO is associated with the ability to donate electrons and is required for the studding of corrosion. It can be seen that as HOMO values increase, so do the inhibitor molecules on the metal surface increase [49]. As a result, research on the mechanism of charge transfer on the metal surface, as well as adsorption, was permitted. Based on the high E_{HOMO} , derivative IIIb have the highest inhibitory activity compared to derivative IIIa which has the lowest inhibitory activity (lower E_{HOMO}). The level of the electron and its ability to accept electrons is referred to as LUMO. Reduced E_{LUMO} values indicate that the inhibitor molecule adds an extra negative charge to the metal's surface.

The LUMO energy level for Both IIIa and IIIb were very closed to each other. It was also discovered that the energy of HOMO and LUMO for inhibitor molecules is higher; as a result, the derivative IIIb inhibitors were discovered to

be reactive by acting as a donor ($-\text{O}-\text{CH}_3$ groups) and anti-corrosion activity. The derivative IIIa inhibitor has the lowest E_{HOMO} and E_{LUMO} values, minimizing metal reactivity and metal donor electrons to the inhibitor. The inhibitor activity has decreased, while the metal's reactivity has increased. According to HOMO-LUMO capacity, Derivative IIIb has the most powerful corrosion inhibition.

The energy gap between E_{HOMO} and E_{LUMO} is important for calculating theoretical inhibitory efficiency for molecular reactivity. It is useful for inhibitor studies to compare ΔE between the two derivatives. The shorter the energy distances, the greater the efficiency of inhibition. The lower value of ΔE in corrosion inhibitors is based on E_{HOMO} rather than E_{LUMO} . Inhibitor derivatives with high HOMO and low ΔE can be used as effective anti-corrosion agents [50]. Because of the increased HOMO energy value and decreasing ΔE , it can be concluded that derivative IIIb would have a strong inhibitory activity, as shown in Fig. 4.

Table 3. Calculated electron identifier using B3LYP/ 6-311G(d,p) for IIIa and IIIb .

Parameters	Equations	Results IIIa	Results IIIb
Total Energy (a.u)		-1978.921	-1888.918

μ (D)		4.1438	5.9823
ELUMO (eV)		-4.47766878	-4.009901376
EHOMO (eV)		-6.294859428	-5.804506396
ΔE (eV)		1.817190648	1.79460502
I	$I = -EHOMO$	6.294859428	5.804506396
A	$A = -ELUMO$	4.47766878	4.009901376
χ (eV)	$\chi = (I + A) / 2$	5.386264104	4.907203886
η (eV)	$\eta = (I - A) / 2$	0.908595324	0.89730251
σ (eV)	$\sigma = 1/\eta$	1.100599985	1.114451357
Pi (eV)	$Pi = -\chi$	-5.386264104	-4.907203886
ω (eV)	$\omega = Pi/2\eta$	15.96521588	13.41835652
ε (eV)	$\varepsilon = Pi \cdot \eta$	-4.893934379	-4.403246364
ΔN	$\Delta N = (\chi_{metal} - \chi_{inhibitor}) / 2 \cdot (\eta_{metal} - \eta_{inhibitor})$	0.888038851	1.166159735

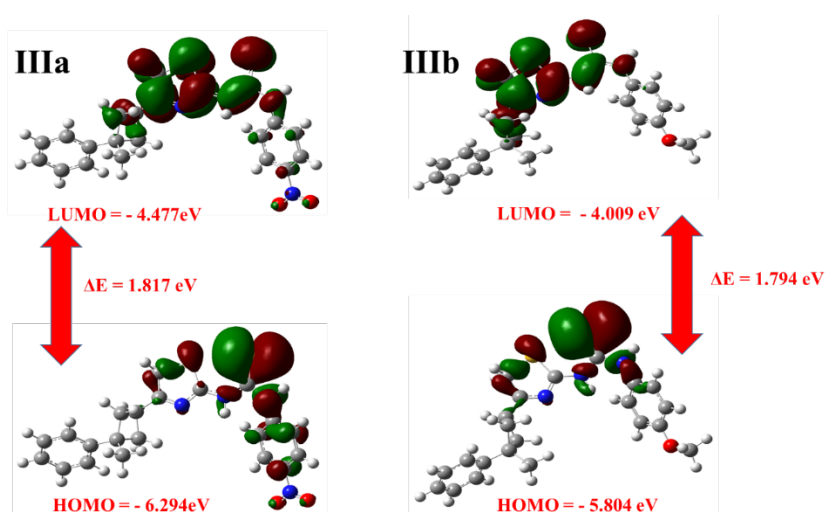
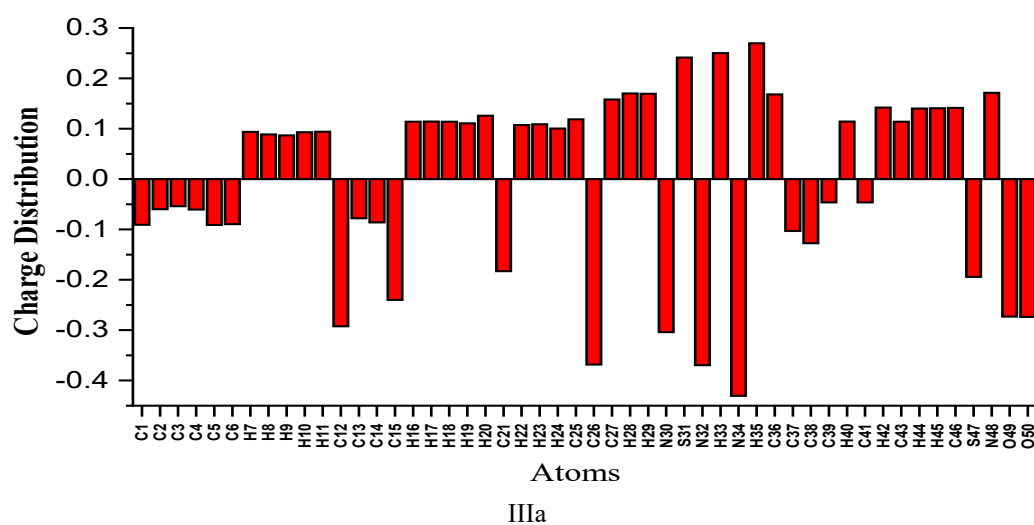
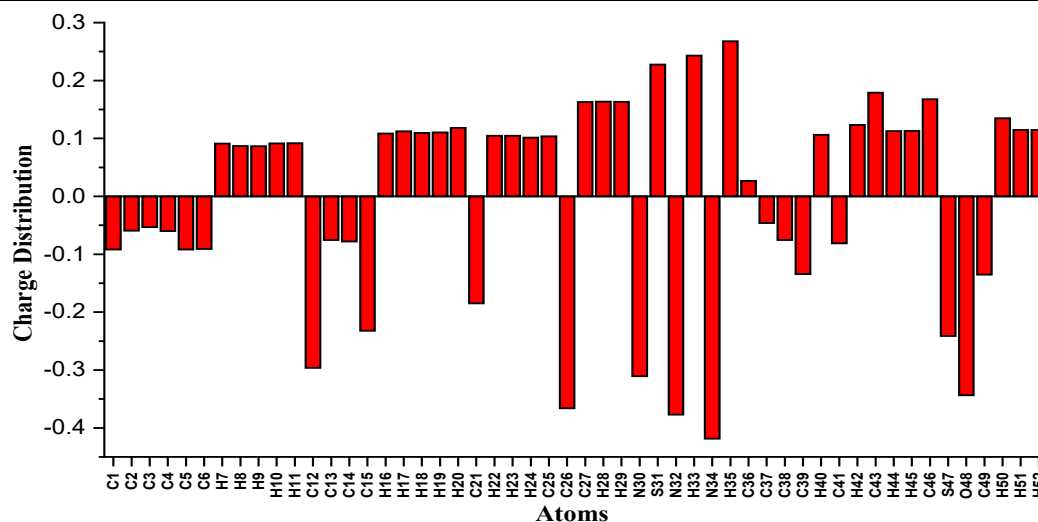


Fig. 4 HOMO and LUMO digram for IIIa and IIIb

Table 4 and Fig. 5 show the charges on the atoms of the derivative's molecular structure. Mulliken methods are widely used to estimate inhibitor adsorption sites [49]. Many researchers have argued that the presence of heteroatoms as a result of the donor-acceptor process has

improved the ability to adsorb on the metal surface [51]. Because of the negatively charged atoms such as N, O, and C atoms in the aromatic ring, derivative IIIb has a more effective inhibitory than derivative IIIa, as shown by the molecular structure and Fig. 5.





IIIb

Fig. 5 Charge distribution on the atoms for both IIIa and IIIb.

Table 4. Millikan charge distribution on the atoms for IIIa and IIIb.

Derivative IIIa		Derivative IIIb	
C1	-0.090794	C1	-0.091644
C2	-0.059986	C2	-0.059331
C3	-0.05375	C3	-0.052965
C4	-0.060348	C4	-0.060022
C5	-0.091146	C5	-0.09172
C6	-0.089634	C6	-0.090682
H7	0.093626	H7	0.091252
H8	0.088569	H8	0.086946
H9	0.086718	H9	0.086624
H10	0.093003	H10	0.091332
H11	0.094003	H11	0.091855
C12	-0.292363	C12	-0.296029
C13	-0.077888	C13	-0.075409
C14	-0.086066	C14	-0.077821
C15	-0.23983	C15	-0.232023
H16	0.114074	H16	0.108615
H17	0.114137	H17	0.112249
H18	0.114067	H18	0.109355
H19	0.110755	H19	0.110445
H20	0.125997	H20	0.118034
C21	-0.182964	C21	-0.184842
H22	0.107274	H22	0.104589
H23	0.10897	H23	0.104678
H24	0.100285	H24	0.101457
C25	0.118509	C25	0.103524
C26	-0.368217	C26	-0.366031
C27	0.158124	C27	0.162827
H28	0.170156	H28	0.163435
H29	0.169553	H29	0.163354
N30	-0.304104	N30	-0.310615
S31	0.241491	S31	0.227451
N32	-0.369658	N32	-0.377073
H33	0.250064	H33	0.242926

N34	-0.430488	N34	-0.418527
H35	0.269796	H35	0.267803
C36	0.168104	C36	0.026579
C37	-0.102938	C37	-0.046082
C38	-0.127347	C38	-0.075432
C39	-0.046303	C39	-0.134237
H40	0.114342	H40	0.106284
C41	-0.046192	C41	-0.081204
H42	0.142061	H42	0.123435
C43	0.113805	C43	0.178995
H44	0.139995	H44	0.112692
H45	0.140776	H45	0.112951
C46	0.141227	C46	0.16775
S47	-0.194069	S47	-0.241094
N48	0.171326	O48	-0.343489
O49	-0.273049	C49	-0.135177
O50	-0.273674	H50	0.134906
		H51	0.114481
		H52	0.114628

Other parameters that can be used to determine an inhibitor's stability, reactivity, and inhibitor activity are η and σ . The σ was greater for derivative IIIb than for derivative IIIa, as shown in Table 3. Because the organic inhibitor used is lewis-based, and soft inhibitors are more reactive than hard inhibitors, they are more effective corrosion inhibitors [58]. The derivative IIIb inhibits with a high E_{HOMO} and a low ΔE , its estimated softness values to be high. The η and σ values have stronger inhibitory effects on derivative IIIb than on derivative IIIa.

The parameters χ and Pi are also used to assess inhibitor activity. The calculated inhibitor, χ values explain how the metal and the inhibitor form a coordinated covalent bond. The corrosion inhibition behavior of iron metal on the inhibitor derivatives. The χ values of the inhibitors in Table 3 were discovered to be less than the value of the iron metal. The iron metal was able to form bonds by absorbing electrons from the inhibitor molecule. The inhibition of derivative IIIb had a lower value of χ and served as the most effective corrosion inhibitor.

Table 3 summarizes the dipole moment (μ) data. According to the literature, there is no direct relationship between μ and inhibition activity. In some studies, the activity of molecules increased with increasing μ value, whereas in others, the inhibition molecule's activity decreased with increasing μ value. The derivative IIIb inhibitor has a higher dipole moment, which can be perceived as a better covering on a metal surface.

The ω and ϵ are important parameters for determining inhibitors to corrosion activities. The ω shows the ability of the inhibitor molecules to accept electrons and ϵ the ability of the inhibitor molecules to donate electrons. Inhibitory activity increases as the ϵ value increases and decreases as the value of ω decreases [52]. In the derivatives of IIIa and IIIb, the ϵ increase in derivatives IIIb and ω has lower than derivative IIIa. Derivative IIIb has a stronger inhibitory effect than derivative IIIa based on ω and ϵ parameters. The ΔN values of derivative IIIb indicate that it is a good inhibitor because the value was

greater than derivative IIIa, implying that more electrons are transferred from organic compound IIIb to the surface of iron metals.

Conclusions

In the first step of this research, new thiazole derivatives (IIIa,b) have been obtained by activating two different isothiocyanate (II) RNCS compounds with 4-(1-Phenyl-1-methyl-cyclobutane-3-yl)-2-aminithiazole (I). Their molecular characterizations were elucidated using IR, ^1H - and ^{13}C - NMR techniques. According to the results, compound IIIb has a higher E_{HOMO} and E_{LUMO} value than compound IIIa. Consequently compound IIIb was determined to be a good donor with high inhibitor activity. Because of the lower ΔE of the compound, IIIb has a stronger inhibitory activity. Furthermore, because it has a higher dipole moment value of IIIb, it can improve metal corrosion resistance. It was discovered that the electronegative atoms have a significant influence on the inhibition action based on the atomic charges of the compound. The distribution of nuclear directions in derivative IIIb indicates that electronegative atoms are thought to impact inhibitory activity significantly. The determined parameters, including η , ω , σ , ϵ , Pi and χ , demonstrated that compound IIIb has a strong corrosion inhibitor effect. A lower χ value for an inhibitor indicates that the iron metal can form a bond by absorbing electrons from the compound inhibitor. The higher the ΔN value, the better the metal surface can be adsorbed, and thus corrosion inhibition can be increased. Finally, both compounds are promising candidates for use as anti-corrosion inhibitors. As the number of heteroatoms in organic structures increased, so did the complexity of the structures; as a result, both derivatives are effective corrosion inhibitors.

Acknowledgments

The author thankfully for Firat University Organic Lab working.

References

1. B. El Ibrahim and L. Guo, Azole-based compounds as corrosion inhibitors for metallic materials. *Azoles-Synthesis, Properties, Applications and Perspectives*, 2020.
2. M.E. Kenari, et al., Enantiomeric separation of new chiral azole compounds. *Molecules*, 2021. 26(1): p. 213.
3. A.M. Abu-Dief, et al., Synthesis and characterization of Fe (III), Pd (II) and Cu (II)-thiazole complexes; DFT, pharmacophore modeling, in-vitro assay and DNA binding studies. *Journal of Molecular Liquids*, 2021. 326: p. 115277.
4. H. Guo, et al., Transition metal-catalysed molecular n-doping of organic semiconductors. *Nature*, 2021. 599(7883): p. 67-73.
5. N. Siddiqui, et al., Diverse biological activities of Thiazoles: A Retrospect. *Int J Drug Dev Res*, 2011. 3(4): p. 55-67.
6. R. Omar, P. Koparir, and M. Koparir, Synthesis of 1, 3-Thiazole derivatives. *Indian Drugs*, 2021. 1: p. 58.
7. M. Miar, et al., Theoretical investigations on the HOMO-LUMO gap and global reactivity descriptor studies, natural bond orbital, and nucleus-independent chemical shifts analyses of 3-phenylbenzo [d] thiazole-2 (3 H)-imine and its para-substituted derivatives: Solvent and substituent effects. *Journal of Chemical Research*, 2021. 45(1-2): p. 147-158.
8. S.H. Ali and A.R. Sayed, Review of the synthesis and biological activity of thiazoles. *Synthetic Communications*, 2021. 51(5): p. 670-700.
9. X.-X. Xie, et al., Synthesis and anticancer effects evaluation of 1-alkyl-3-(6-(2-methoxy-3-sulfonylamino-pyridin-5-yl) benzo [d] thiazol-2-yl) urea as anticancer agents with low toxicity. *Bioorganic & Medicinal Chemistry*, 2015. 23(19): p. 6477-6485.
10. A. Prakash and D. Adhikari, Application of Schiff bases and their metal complexes-A Review. *Int. J. Chem. Tech. Res*, 2011. 3(4): p. 1891-1896.
11. W. Zopubi, Biological activities of Schiff bases and their complexes: a review of recent work. *Int. J. Org. Chem*, 2013. 3: p. 73-95.
12. H. Kunkely and A. Vogler, Photochemistry of N, N'-bis (3, 5-di-tert-butylsalicylidene)-1, 2-diaminocyclohexane and its Co (II) complex in chloroform. *Journal of Photochemistry and Photobiology A: Chemistry*, 2001. 138(1): p. 51-54.
13. S.H. Rahaman, et al., Synthesis, structure and properties of mononuclear cobalt (II) and cobalt (III) pseudohalide complexes containing N-donor Schiff bases: Synthetic control of metal oxidation levels. *Polyhedron*, 2005. 24(13): p. 1755-1763.
14. N. Gümrükçüoğlu, et al., Determination of stability constants of triazole ligand carrying naphthol group with heavy metal ions in aqueous solutions. *Pakistan Journal of Analytical & Environmental Chemistry*, 2013. 14(2): p. 7.
15. J. Li, et al., Recent advances in the total synthesis of cyclobutane-containing natural products. *Organic Chemistry Frontiers*, 2020. 7(1): p. 136-154.
16. V.M. Dembitsky, Naturally occurring bioactive Cyclobutane-containing (CBC) alkaloids in fungi, fungal endophytes, and plants. *Phytomedicine*, 2014. 21(12): p. 1559-1581.
17. T. Seiser, et al., Cyclobutanes in Catalysis. *Angewandte Chemie International Edition*, 2011. 50(34): p. 7740-7752.
18. P. KOPARIR, et al., Synthesis, Characterization, and theoretical inhibitor study for (1E, 1'E)-2, 2'-thiobis (1-(3-mesityl-3-methylcyclobutyl) ethan-1-one) dioxime. *El-Cezeri*, 2020. 8(3): p. 1495-1510.
19. O. Rebaz, et al., Theoretical Determination of Corrosion Inhibitor Activities of Naphthalene and Tetralin. *Gazi University Journal of Science*, 2022. 35(2): p. 434-444.
20. L. AHMED and O. Rebaz, 1H-Pyrrole, Furan, and Thiophene Molecule Corrosion Inhibitor Behaviors. *Journal of Physical Chemistry and Functional Materials*. 4(2): p. 1-4.
21. A. Patel, et al., Impedance spectroscopic study of corrosion inhibition of Al-Pure by organic Schiff base in hydrochloric acid. *Journal of Saudi Chemical Society*, 2013. 17(1): p. 53-59.
22. O. Rebaz, et al., Structure reactivity analysis for Phenylalanine and Tyrosine. *Cumhuriyet Science Journal*, 2021. 42(3): p. 576-585.
23. R. Sure and S. Grimme, Corrected small basis set Hartree-Fock method for large systems. *Journal of computational chemistry*, 2013. 34(19): p. 1672-1685.
24. L. Türker, et al., A DFT study on nitrotriazines. *Journal of Hazardous Materials*, 2009. 167(1-3): p. 440-448.
25. R.A. OMER, et al., Computational and spectroscopy study of melatonin. *Indian Journal of Chemistry-Section B (IJC-B)*, 2021. 60(5): p. 732-741.
26. R.A. Omer, et al., Theoretical analysis of the reactivity of chloroquine and hydroxychloroquine. *Indian Journal of Chemistry-Section A (IJCA)*, 2020. 59(12): p. 1828-1834.
27. X. Li, S. Deng, and H. Fu, Three pyrazine derivatives as corrosion inhibitors for steel in 1.0 M H₂SO₄ solution. *Corrosion science*, 2011. 53(10): p. 3241-3247.
28. P. Koparir, K. Sarac, and R.A. Omar, Synthesis, molecular characterization, biological and computational studies of new molecule contain 1, 2, 4-triazole, and Coumarin bearing 6, 8-dimethyl. *Biointerface Research in Applied Chemistry*, 2022. 12(1): p. 809-823.
29. M. Karelson, V.S. Lobanov, and A.R. Katritzky, Quantum-chemical descriptors in QSAR/QSPR studies. *Chemical reviews*, 1996. 96(3): p. 1027-1044.
30. J. Fang and J. Li, Quantum chemistry study on the relationship between molecular structure and corrosion inhibition efficiency of amides. *Journal of Molecular Structure: THEOCHEM*, 2002. 593(1-3): p. 179-185.
31. O. Rebaz, et al., Computational determination the reactivity of salbutamol and propranolol drugs. *Turkish Computational and Theoretical Chemistry*, 2020. 4(2): p. 67-75.
32. L.J. Bartolotti and K. Flurchick, An introduction to density functional theory. *Reviews in computational chemistry*, 1996. 7: p. 187-260.
33. L. AHMED and O. Rebaz, Spectroscopic properties of Vitamin C: A theoretical work. *Cumhuriyet Science Journal*, 2020. 41(4): p. 916-928.
34. R.A. Omer, P. Koparir, and L.O. Ahmed, Characterization and Inhibitor Activity of Two Newly

Synthesized Thiazole. *Journal of Bio-and Tribo-Corrosion*, 2022. 8(1): p. 1-12.

35. M.G.K. AlFalah and F. Kandemirli, Corrosion inhibition potential of dithiohydrazodicarbonamide derivatives for mild steel in acid media: synthesis, experimental, DFT, and Monte Carlo studies. *Arabian Journal for Science and Engineering*, 2021: p. 1-30.

36. R. Dennington, T. Keith, and J. Millam, GaussView, version 5. 2009.

37. L. AHMED and O. Rebaz, The Role of the Various Solvent Polarities on Piperine Reactivity and Stability. *Journal of Physical Chemistry and Functional Materials*. 4(2): p. 10-16.

38. A.D. Becke, Density-functional thermochemistry. IV. A new dynamical correlation functional and implications for exact-exchange mixing. *The Journal of chemical physics*, 1996. 104(3): p. 1040-1046.

39. D. Bálint and L. Jäntschi, Comparison of molecular geometry optimization methods based on molecular descriptors. *Mathematics*, 2021. 9(22): p. 2855.

40. T. Koopmans, Über die Zuordnung von Wellenfunktionen und Eigenwerten zu den einzelnen Elektronen eines Atoms. *physica*, 1934. 1(1-6): p. 104-113.

41. B.N. Plakhutin and E.R. Davidson, Koopmans' theorem in the restricted open-shell Hartree–Fock Method. 1. A variational approach. *The Journal of Physical Chemistry A*, 2009. 113(45): p. 12386-12395.

42. E.P. Jesudason, et al., Synthesis, pharmacological screening, quantum chemical and in vitro permeability studies of N-Mannich bases of benzimidazoles through bovine cornea. *European journal of medicinal chemistry*, 2009. 44(5): p. 2307-2312.

43. H. Gökce and S. Bahçeli, A study on quantum chemical calculations of 3-, 4-nitrobenzaldehyde oximes. *Spectrochimica Acta Part A: Molecular and Biomolecular Spectroscopy*, 2011. 79(5): p. 1783-1793.

44. M. Arivazhagan and V. Subhasini, Quantum chemical studies on structure of 2-amino-5-nitropyrimidine. *Spectrochimica Acta Part A: Molecular and Biomolecular Spectroscopy*, 2012. 91: p. 402-410.

45. M.S. Masoud, et al., Synthesis, computational, spectroscopic, thermal and antimicrobial activity studies on some metal–urate complexes. *Spectrochimica Acta Part A: Molecular and Biomolecular Spectroscopy*, 2012. 90: p. 93-108.

46. S.-i. Kiyooka, D. Kaneno, and R. Fujiyama, Parr's index to describe both electrophilicity and nucleophilicity. *Tetrahedron Letters*, 2013. 54(4): p. 339-342.

47. R.G. Pearson, Absolute electronegativity and hardness: application to inorganic chemistry. *Inorganic chemistry*, 1988. 27(4): p. 734-740.

48. A.Y. Musa, R.T. Jalgham, and A.B. Mohamad, Molecular dynamic and quantum chemical calculations for phthalazine derivatives as corrosion inhibitors of mild steel in 1 M HCl. *Corrosion Science*, 2012. 56: p. 176-183.

49. S. Chen, et al., Quantum chemical study of some benzimidazole and its derivatives as corrosion inhibitors of steel in HCl solution. *Int. J. Electrochem. Sci*, 2014. 9: p. 5400-5408.

50. M. Beytur, et al., Synthesis, characterization and theoretical determination of corrosion inhibitor activities of some new 4, 5-dihydro-1H-1, 2, 4-Triazol-5-one derivatives. *Heliyon*, 2019. 5(6): p. e01809.

51. Z. El Adnani, et al., DFT theoretical study of 7-R-3methylquinoxalin-2 (1H)-thiones (RH; CH₃; Cl) as corrosion inhibitors in hydrochloric acid. *Corrosion Science*, 2013. 68: p. 223-230.

52. N. Karakus and K. Sayin, The investigation of corrosion inhibition efficiency on some benzaldehyde thiosemicarbazones and their thiole tautomers: Computational study. *Journal of the Taiwan Institute of Chemical Engineers*, 2015. 48: p. 95-102.